



## Development of highly porous carbon nanocomposites derived from coconut shell and its in vitro efficacy of ochratoxin A detoxification

Naila Gulfam<sup>a</sup>, Muhammad Khisroon<sup>a</sup>, Muhammad Zahoor<sup>b,\*</sup>, Farhat Ali Khan<sup>c</sup>

<sup>a</sup>Department of Zoology, Peshawar University, Khyber Pakhtunkhwa, Pakistan, email: nailazoo@yahoo.com (N. Gulfam), m\_khisroon@upesh.edu.pk (M. Khisroon)

<sup>b</sup>Department of Chemistry, University of Malakand, Chakdara, Dir Lower, 18800 KPK, Pakistan, email: mohammadzahoorus@yahoo.com (M. Zahoor)

<sup>c</sup>Principal Abbotabad International College of Pharmacy AIMI, Abbotabad, KPK, Pakistan, email: farhatkhan2k9@yahoo.com (F.A. Khan)

Received 16 August 2017; Accepted 1 February 2018

### ABSTRACT

The current study involves the preparation of highly porous carbon based nanocomposites from coconut shell in specially designed chamber. The prepared adsorbent was characterized through SEM, XRD, TG/DTA, SAA and FTIR. The adsorbent exhibited high surface area (217.06 m<sup>2</sup>/g) and the presence of magnetic iron oxide in the composite structure was evident from SEM, FTIR, EDX and XRD images. Freundlich and Langmuir isotherms were used for determining adsorption parameter of the prepared adsorbent. The equilibrium time for ochratoxin A adsorption on prepared adsorbent from coconut shell at pH 7 was 240 min. The value of  $\Delta S^\circ$  (82 KJ·mol<sup>-1</sup>·deg<sup>-1</sup>) was positive while the values of  $\Delta H^\circ$  (–21 KJ·mol<sup>-1</sup>) and  $\Delta G^\circ$  (–2.75, –3.57, –4.39 and –5.21 KJ·mol<sup>-1</sup> at 30, 40, 50 and 60°C correspondingly) were negative. The negative value  $\Delta H^\circ$  shows that the adsorption process is exothermic and increased negative values of  $\Delta G^\circ$  with temperature demonstrated that the adsorption process was favorable at high temperature.

*Keywords:* Ochratoxin A; Characterization; Adsorption parameters; Coconut shell

### 1. Introduction

Mycotoxins are the secondary metabolites of toxigenic fungi which are unavoidable contaminants in feeds and foods, bringing about injurious effects upon animal and human health [1]. Zearalenone, deoxynivalenol, T-2 toxin, aflatoxins, fumonisins and ochratoxins are the frequently occurring fungal toxins in naturally contaminated feeds and foods [2]. The fungal strains of genus *Aspergillus* and *Penicillium* like *Aspergillus ochraceus*, *Aspergillus niger*, *Aspergillus carbonarius* and *Penicillium verocosum* produce ochratoxin [1].

Structurally, all the ochratoxins consist of derivatives of polyketide dihydrocoumarin moiety linked through the 7-carbon group to L- $\beta$ -phenylalanine by an amide bond [2]. The contamination of ochratoxin A in pre- and post-harvest management is widespread and is extensive one as com-

pared to other mycotoxins contaminations in poultry feed. The contamination prevalence of ochratoxin A is even high when the environmental conditions are favorable for fungal growth (high moisture contents in feed). The presence of ochratoxin A can be confirmed in food products even in the absence of visible mould as well [3]. There is an increasing interest in the development and application of feasible techniques for control of mycobiota and detoxification of their toxin in feed and food. Various chemical, physical and biological measures and treatments have been taken into account for ochratoxin detoxification [4]. Application of adsorbents for the treatment of mycotoxicosis in animals and poultry birds is one of the effective methods [5].

Activated carbon due to its high surface area is widely used for the removal of organic and inorganic contaminants from water. However, the high cost of commercial activated carbon has compelled the researchers to prepare the efficient activated carbon with minimum price and

\*Corresponding author.

from such materials that are available abundantly. The waste biomass have been used by many authors for the preparation of activated carbon [6,7]. The other problem associated with activated carbon is its light weight due to which its settling time in reactors is high. To remove this discrepancy, a number of authors have attempted to render it magnetic which can then be easily removed from slurry after treatment through magnetic process. Unfortunately magnetic oxides deposition on activated carbon considerably decreases its surface area [8]. In order to solve this problem the present study was aimed to prepare highly porous magnetic nanocomposites from coconut shell and to analyze its in vitro efficacy of detoxification of ochratoxin A.

## 2. Material and methods

### 2.1. Preparation of highly porous carbon based nanocomposite

Preparation of adsorbent was carried by following the method of Khan et al. [9] with slight modification. Coconut shell was utilized as bulk material for preparation of carbon based adsorbents. The material was crushed and soaked in ethanolic  $\text{FeCl}_3 \cdot 6\text{H}_2\text{O}$  (10% w/v). After 30 min, the biomass was taken out and shade dried for about 24 h at room temperature. The dried material was then passed through pyrol fumigation for 48 h for pyrolysis. The pyrol treated material was further shifted to oven for drying at 100°C for 5 h. After that the sample was charred in a specially designed chamber consisting of electric heater, wire gauze, inlet, exhaust outlet and supply of nitrogen gas (to provide inert environment). Temperature in the chamber was 500°C, which was achieved in such a manner that there was 10°C increase in temperature/min. The partially treated material was kept in the chamber for 2 h to accomplish the process. A magnetic bar was also used to note its magnetic property. When the produced sample was subjected to magnetic bar, all the sample contents stick to it. This clearly indicated that formation of Iron oxide has occurred. After iron oxide carbon nanocomposites were produced, it was treated with different concentrations of  $\text{HNO}_3$  solution for 75 min. Excess of Iron oxide was released by acid treatment and porosity was enhanced in Iron oxide carbon based nanocomposites. After treatment with acid the composite was subjected to bar magnet.

### 2.2. Characterization of nanocomposites

The prepared Iron oxide carbon nanocomposite was then characterized by different instrumental techniques like SEM, XRD, TG/DTA, SAA and FTIR.

The SEM analyses of the detectable features of samples were done by putting the sample on SEM grid and gold coated through sputter coater (SPI, USA) at 30 mA for 2 min. The images were then taken by Joel JSM-5910 SEM at an accelerating voltage of 20 KV.

XRD analyses was carried out using Joel X-ray diffractometer, JDX-3532 (current = 2.5–80 mA, voltage = 20–60 kV, X-rays = Cu  $K\alpha$ ,  $2\theta = -3$  to 160°). The analyses of sample was carried by XRD with Ni filter, using monochromatic Cu

$K\alpha$  radiation of 1.5418Å° wave length. The X-ray generator was switched on at 40 kV and 30 mA. The scanning range  $2\theta/\theta$  and scanning speed 10  $\text{min}^{-1}$  were employed for precise determination.

Elemental composition of the prepared highly porous carbon based adsorbent was determined by using EDX linked with SEM JSM-5910 (JEOL, Japan) model INCA 200 X-sight Oxford Instrument U.K. The dispersed particles were placed on both sides of adhesive tape and then placed on stub of microscope made up of aluminum.

TG/DTA of the prepared highly porous carbon based adsorbent was done by Diamond Series TG/DTA Perkin Elmer, USA analyzer using  $\text{Al}_2\text{O}_3$  as reference.

The quality and utility of material are determined by two important physical parameter including surface area and porosity. The variations in the porosity and surface area of adsorbent material influence its performance to a great extent. About 0.1 g of iron oxide carbon based adsorbent was taken and analyzed by Surface Area Analyzer (NOVA 2200e Quantachrome, USA) using  $\text{N}_2$  as purge gas.

The IR spectra of the prepared sample were obtained by using IR Prestige-21, Shimadzu Japan. The scanning of the prepared sample was carried in the range of 750–525  $\text{cm}^{-1}$  and 4000–600  $\text{cm}^{-1}$ .

### 2.3. Determination of kinetics parameters

The kinetics of ochratoxin A adsorption was carried out in line with the approach of Stroka et al. [10]. To determine the equilibrium time of adsorption and best kinetics model, a series of 25 mL flasks were taken and 5.4 mL ethanol and 13 mL distilled water (pH 7) were poured in it. Each flask was spiked with known quantity of standard ochratoxin A (400 ppm = 400  $\text{mg}\cdot\text{L}^{-1}$ ). Then the prepared adsorbent was put into flasks to attain 0.5% w/v concentration of adsorbent in each flask. Rotation of these flasks was carried at 300 rpm and room temperature for different time intervals. Separation of sorbents was carried out using Watman No-1 filter for each period time. The remaining concentrations of the adsorbate were determined using HPLC (Hitachi model L-200).

### 2.3. Ochratoxin quantification by HPLC system

Quantification of ochratoxin A was carried out by using HPLC system (Hitachi model L-200) with two pumps L-2130, automobile injector L-2200 and fluorescence detector L-2458 (Macoa, Japan). Through sonication degassing of the mobile phase was carried (acetonitrile/methanol/normal water at the ration of 8:27:65, v/v/v). The column inter-sil ODS-3 (25 cm × 4.5 mm I.D., 5 nm, GL knowledge, Tokyo, Japan) was linked as LC column and retained at 40°C. The injecting volume was 20  $\mu\text{l}$  with rate of flow of 0.8 mL/min. The ochratoxin A was detected at the wavelengths of 365 and 450 nm (excitation and emission), respectively.

### 2.4. Determination of adsorption parameters

A series of flasks were prepared to obtain the required concentrations of 150, 175, 200, 225, 250, 275, 300, 325, and 350 ppm. All the flasks were shaken at 300 rpm for 450

min at room temperature. After separation of adsorbent the solution were subjected to HPLC analyses as described above.

### 2.5. Determination of the effect of pH on adsorption

A series of 25 mL flasks were prepared to optimize pH for ochratoxin A adsorption. The range of pH was kept from 1–14 and spiked with standard ochratoxin A to attain concentration of 400 ppm before adding to sorbent. All the flasks were rotated at 300 rpm for 450 min. Then the sorbent was separated and LC analyses was carried out as described above.

### 2.6. Effect of temperature on adsorption

Adsorption experiments on ochratoxin A (400 ppm) solutions were conducted at 30, 40, 50, and 60°C for 450 min. Then the adsorbent was removed and the subsequent concentrations of contaminant were determined as mentioned above.

## 3. Results and discussion

### 3.1. Prepared and characterization of nanomaterials

#### 3.1.1. Characterization by surface area analyzer

The surface parameters of highly porous carbon nanocomposite prepared from coconut shell is presented in Table 1. The prepared adsorbent exhibited comparable surface area (217.06 m<sup>2</sup>/g) with micro pore volume of 1.30 cm<sup>3</sup>/g, total pores volume of 3.71 cm<sup>3</sup>/g and average pore diameter of 65.31 Å.

It has been claimed that the surface area of the carbon nanocomposite can be increased up to 2500 m<sup>2</sup>/g through chemical or physical activation [11]. Zhang et al. [11] prepared highly porous carbon from rice straw and corn stalks after chemical activations and observed increase in surface area due to activation. The surface area reduction due to iron oxide deposition has already been reported by Khan et al. [12]. Muhammad et al. [13] reported the surface area parameters of the iron oxide carbon nano-structures prepared from biomass. It has been noted that the values of surface area, total pores volume and micropore volume were very less as compared to our results. The surface area reported in this paper is less as compared to commercially available activated carbon. If we look to iron oxide composites surface area in literature, then it is comparatively high

and its reason is that we have removed 50% of the deposited iron oxide through nitric acid treatment in order to increase the surface area.

#### 3.1.2. SEM analyses

SEM was used to investigate the morphology of Iron oxide carbon nanocomposites (Fig. 1). Through SEM technique, it is possible to observe the surface defects of the material [14,15]. The white patches of Iron oxide are clearly seen in the pictograph whereas the black area representing the carbon. The SEM picture also indicated the over deposition of Iron oxide on the surface of carbon.

Although a number of researchers have prepared magnetic carbon nanocomposites, for example Jorge et al. [16] developed magnetic carbon nanocomposite and particle sizes of Iron oxide were noted ranging between 8.0 to 22 nm. Similar studies were also conducted by Zahoor and Khan [8] in which they prepared Iron oxide nanocomposite from bagasse and maize straw and used for the detoxification of aflatoxin B1. Muhammad et al. [8,13] develop Magnetic carbon nanostructures from water melon and melon waste and used for the removal of heavy metals from water. As depicted from Fig. 1 the iron oxide over deposition causes reduction in surface area of composites. None of the researchers have tried to enhance the surface area of the composites. As the prepared composite contains iron oxide as integral component and its deposition on activated carbon surface has decreased the surface area, so in order increase the surface area and retain the magnetic character as well, the prepared composites were treated with different acid concentration solutions for 75 min. 0.01 N acid solution was found optimum as at higher concentrations the total removal of the iron oxide components were observed which was not desirable as for magnetic application iron oxide is needed. In the present study an attempt have been carried out to enhance porosity of the prepared composites by treating it with 0.01 N HNO<sub>3</sub> solution for 75 min.

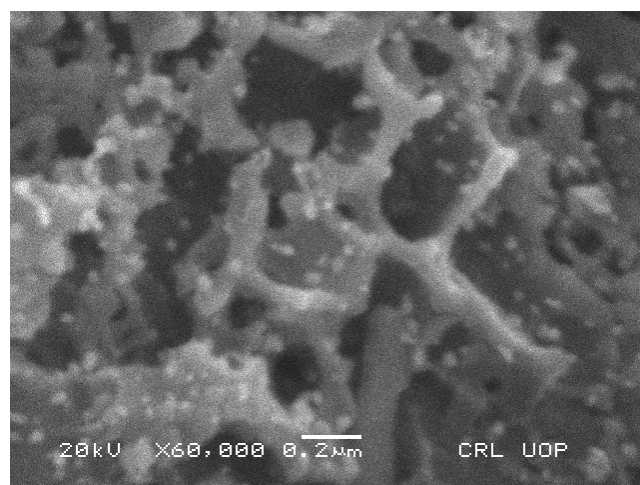


Fig. 1. SEM pictograph of the prepared Iron oxide carbon nanostructure prepared from coconut shell.

Table 1  
Surface characteristics of highly porous carbon nanocomposite prepared from coconut shell

Physical properties	Values
BET surface area, m <sup>2</sup> /g	217.06
Langmuir surface area, m <sup>2</sup> /g	989.12
Total pore volume, cm <sup>3</sup> /g	3.71
Micropore volume, cm <sup>3</sup> /g	1.30
Average pore diameter, Å	65.31

Fig. 2 displays an overview of the Iron oxide carbon nanocomposite after treating with  $\text{HNO}_3$ . The enhanced porosity is evident from its honeycomb like porous surface which confirms that the excess of deposited iron oxide has been removed by  $\text{HNO}_3$ . However it should be noted that concentrated  $\text{HNO}_3$  will totally remove the deposited iron oxide on the surface of composite. The presence of iron oxide on the surface of the composite is needed, as the settling time of activated carbon in the reactor are quite high and if magnetic oxide is deposited on it, can easily be removed after treatment from slurry by magnetic process. So its total removal from composite surface is not desired. To optimize the  $\text{HNO}_3$  concentration the adsorbent was treated with different concentrations of  $\text{HNO}_3$  solution and after 75 min it was subjected to magnet bar. The concentration of  $\text{HNO}_3$ , 0.01 N was found to be optimum. At this concentration the composite was attracted actively by magnet and also it is evident from the white patches in the SEM image as given in Fig. 2.

### 3.1.3. XRD analyses

The XRD analyses of highly porous carbon nanocomposite prepared from coconut shell (Fig. 3) shows that the composite contains crystalline iron oxide on its surface. The diffraction peaks at  $2\theta$ ; 17.65, 30.15, 35.50, 37.45, 53.50, 57.10 and 62.35 represent the corresponding indices of 111, 220, 311, 222, 422, 511 and 440 representing magnetite as reported by Zahoor et al. [8] and Muhammad et al. [13]. Diffraction peaks at  $2\theta$ ; 11.30, 22.30, 33.05, 37.45, 40.80, 42.45, 45.20, 50.55, 53.95, 57.17 and 61.40 represents the corresponding indices; 020, 110, 130, 200, 121, 140, 131, 211, 221, 151 and 250 which confirms the presence of  $\alpha$ -FeOOH (goethite) [17,18], whereas the diffraction peaks at  $2\theta$ ; 23.95 and 49.35 corresponds to indices of 012 and 024 representing  $\alpha$ - $\text{Fe}_2\text{O}_3$  (hematite) [17].

The presence of Iron oxide in nanocages has also been reported by Hengfei et al. [19]. A similar study of developing highly porous carbon from bamboo was carried out by Wan et al. [20] using chemical process. However the

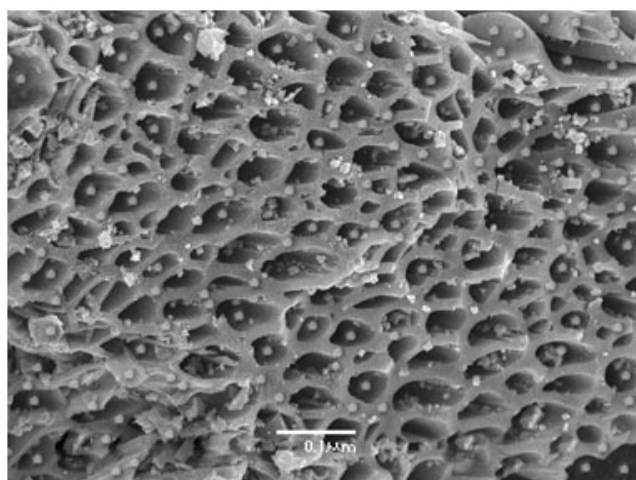


Fig. 2. SEM pictograph of highly porous carbon nanocomposite prepared from coconut shell.

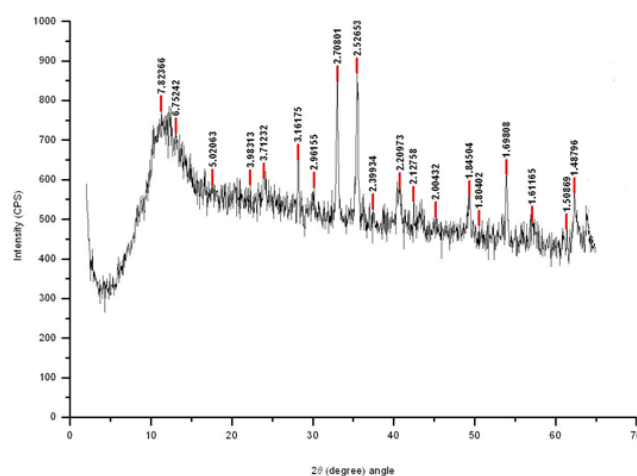


Fig. 3. XRD pattern of highly porous carbon nanocomposite prepared from coconut shell.

reported XRD spectra showed amorphous nature of the prepared porous carbon from bamboo, representing the complete loss of iron oxide component in porosity development. In the study of Al-Qodah et al. [21] the disappearance of Iron oxide was observed when the iron oxide carbon nanocomposite were treated with  $\text{HNO}_3$  solution. They attempted to enhance the porosity of the composite. Amorphous nature of the resulting granular activated carbon composite was evident from their XRD pattern. Deng et al. [22], studied the carburized cotton fabric and observed the XRD spectrum indicating the amorphous nature of the analyzed sample.

### 3.1.4. Characterization by EDX

The highly porous carbon nanocomposite prepared from coconut shell was characterized by Energy Dispersive X-ray. Fig. 4 represents the elemental composition of composite. The EDX pattern shows the presence of carbon, oxygen and iron. The iron is present at 0.7, 2.6, 6.5 and 7 KeV indicating iron oxide is still there in the composite structure.

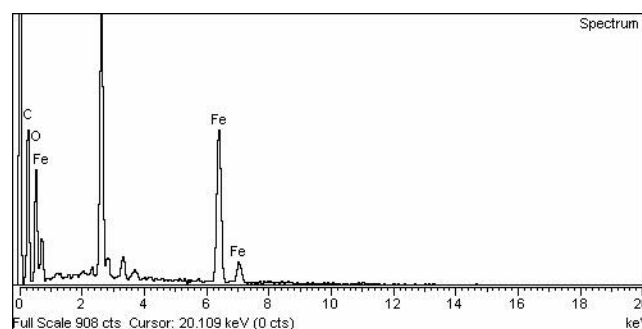


Fig. 4. EDX spectra of the highly porous carbon nanocomposite prepared from coconut shell.

Hengfei et al. [19] analyzed the magnetic carbon nanocages through EDX and reported the presence of Iron oxide in the composite. The EDX technique has been widely used to identify metals and/or contaminants in nanocomposites. Kahani et al. [9] used this technique to verify the presence or absence of contaminants in carbon nanotubes. Jorg et al. [16] represented the EDX spectra of activated carbon and concluded the absence of Fe peaks at deferent level of KeV that showed the amorphous properties of activated carbon. According to Hengfei et al. [19] the magnetic carbon nanocages after treatment with acid showed a very small peak at 6.4 KeV, however the other intense peaks of Fe were disappeared. The appearance small peak at 6.4 KeV may be due to the remaining of Fe particles in carbon nanocages after acid treatments. In our study we have optimized the  $\text{HNO}_3$  concentration and at this concentration all the iron peaks can be observed.

### 3.1.5. Characterization by TG/DTA

The decrease in mass of the prepared nanostructures was observed at different temperature. Fig. 5 represents the thermogravimetric and differential thermal analyses of highly porous carbon nanocomposite prepared from coconut shell. TG graph indicates gradual loss of weight up to 390°C. An abrupt fall in loss of weight was noted from 400 to 595°C, whereas no loss of weight was observed above 600°C. In DTA graph, two endothermic peaks at 340 and 540°C were observed representing that maximum heat was absorbed by the prepared sample at these points. However two exothermic peaks were also present at 430 and 610°C that are the signs of maximum loss of mass at these two stages.

In our previous work we prepared Iron oxide carbon nanocomposite from bagasse and water melon wastes [8,13]. The prepared composites were analyzed by TG/DTA. Similar weight loss at two different points with two endothermic peaks were observed. However the temperatures at which the endothermic peaks were observed were different.

### 3.1.6. Characterization by FTIR

FTIR is mainly used to measure the quality of analyzed sample and thus can provide basic information on the

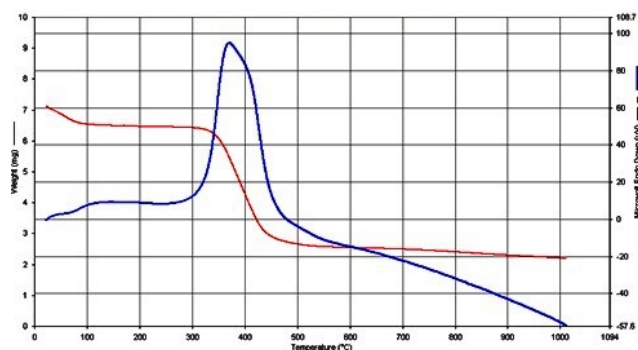


Fig. 5. TG/DTA spectra of the highly porous carbon nanocomposite prepared from coconut shell.

molecular structure of organic or inorganic compounds. IR spectroscopy is therefore a powerful technique which makes available fingerprint data on the chemical composition of the sample [23]. The mid and far IR spectra of highly porous carbon nanocomposite prepared from coconut shell are presented in Figs. 6 and 7. The FTIR spectrum exhibit band at 3412  $\text{cm}^{-1}$  showing stretching vibration of O-H whereas 2600  $\text{cm}^{-1}$  representing the aliphatic C-H. The bands between 1800 to 1600  $\text{cm}^{-1}$  can be attributed to C=O and C=C respectively [20]. Other significant bands at 1002.98 and 1130  $\text{cm}^{-1}$  are ascribed to C-O stretching as reported in earlier studies [24]. The band at 587  $\text{cm}^{-1}$  (Fig. 6) correspond to stretching of Fe-O deposited in the pores and surface of the prepared adsorbent as reported by Sneha et al. [25] and Mohammad et al. [8].

### 3.2. Adsorption isotherm

By means of Giles isotherm [26], the adsorption capacity of the synthesized adsorbent towards ochratoxin A was

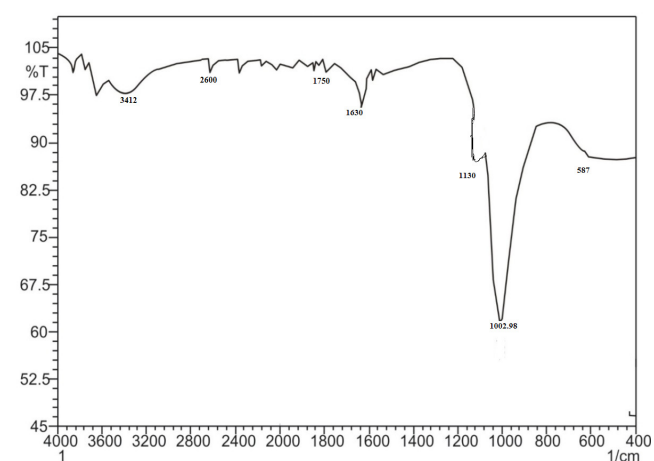


Fig. 6. Mid IR spectra of the highly porous carbon nanocomposite derived from coconut shell.

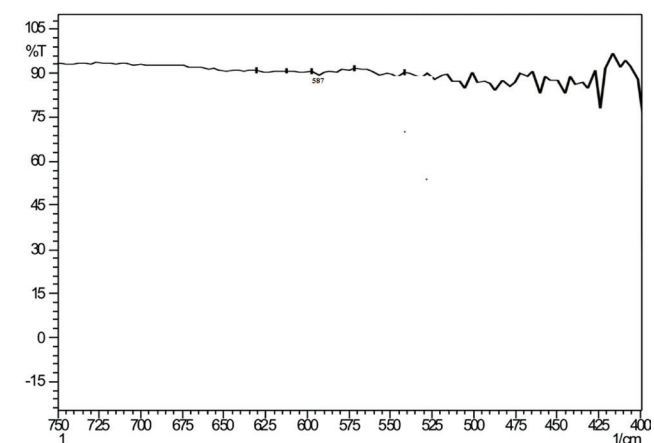


Fig. 7. Far IR spectra of the highly porous carbon nanocomposite derived from coconut shell.

determined. The plot of concentration (C) versus amount of ochratoxin A adsorbed (q) is presented in Fig. 8. On the basis of curvature and initial slope, Giles classify the isotherms into; high affinity (H), constant partition (C), sigmoidal (S) and Langmuir (L) categories. Isotherms in Fig. 8 is C type. C type isotherms are characterized by the constant partition of contaminant between solution and substrate up to maximum possible adsorption. It also indicated that the number of adsorption sites remains persistent and more sites are produced with the advancement of adsorption process that is indicated by linearity of the curve. This is the case where maximum attraction of solute, rather than solvent persists for adsorbent. The solute then breaks, enters the substrate bonds thereby interfering with penetration of solvent.

Langmuir [27] and Freundlich [28] adsorption isotherms were used to quantify the adsorption potential of ochratoxin A on the adsorbents prepared from coconut shell. The linear form of Langmuir equation is given as follows:

$$\frac{c}{q} = \frac{c}{Q_0} - \frac{1}{Q_0 b} \tag{1}$$

In this equation, the amount of ochratoxin A adsorbed (mg g<sup>-1</sup>) is represented by q, equilibrium concentration of ochratoxin A (mg L<sup>-1</sup>) is represented by C, whereas b and Q<sub>0</sub> are constants of Langmuir equation. The energy of the process is represented by b while maximum adsorption capacity of the adsorbent is indicated by Q<sub>0</sub>. The plots of equilibrium concentration (C) against specific adsorption (C/q) are presented in Fig. 9.

The values of Langmuir constants (b and Q<sub>0</sub>) were obtained from the slope and intercept of the plot given in Fig. 9 and were found to be 0.181 mg g<sup>-1</sup> and 177.6 mg g<sup>-1</sup> respectively while R<sup>2</sup> value was 0.985 (Table 2). The adsorption capacity of this adsorbent is high as compared to the other nanocomposites that we have used in our previous studies [8,13].

Heterogeneous system is generally described by using Freundlich isotherm that is represented by the equation given below:

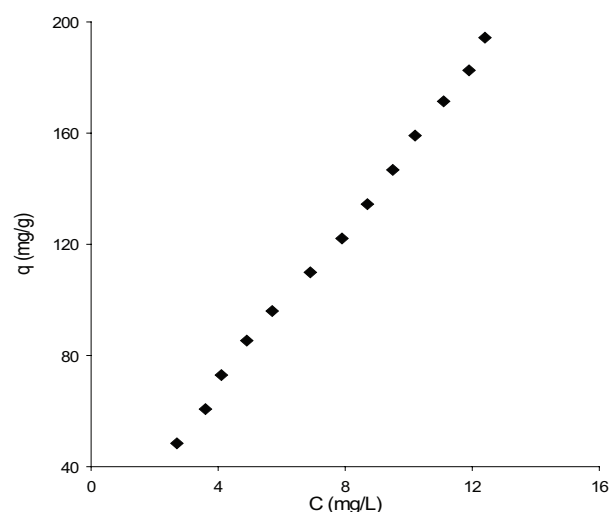


Fig. 8. Giles isotherm of ochratoxin A adsorption on highly porous iron oxide carbon nanocomposite derived from coconut shell.

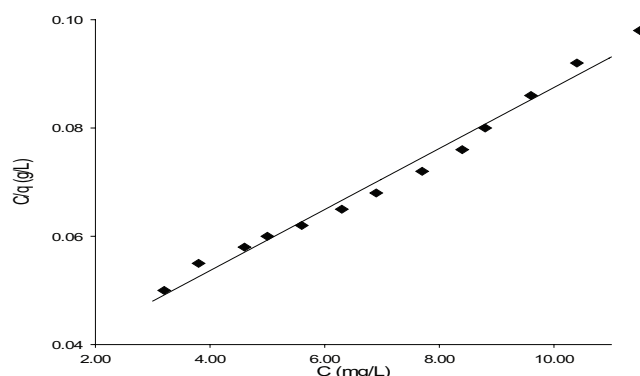


Fig. 9. Langmuir plot of ochratoxin A adsorption on highly porous iron oxide carbon nanocomposite derived from coconut shell.

Table 2  
Isotherm parameters for ochratoxin A adsorption on iron oxide carbon nanocomposite derived from coconut shell

Adsorbent prepared from	Langmuir isotherm			Freundlich isotherm		
	Q <sub>0</sub> (mg g <sup>-1</sup> )	b	R <sup>2</sup>	K	1/n	R <sup>2</sup>
Coconut shell	177.6	0.181	0.985	25.2	0.773	0.997

$$\ln q = \ln K + \frac{1}{n} \ln C \tag{2}$$

The equilibrium concentration is represented by (C) with a unit of mg L<sup>-1</sup>, the total amount of ochratoxin A adsorption (mg g<sup>-1</sup>) is represented by q, while K and n are constants of Freundlich equation, K shows the adsorption capacity whereas n denotes the intensity of the adsorption.

The values of Freundlich constants K and 1/n were obtained from the slope and intercept of the ln C versus ln q plot for the prepared adsorbent (Fig. 10) and were found to be 25.2 and 0.773 respectively, with R<sup>2</sup> value of 0.997 (Table

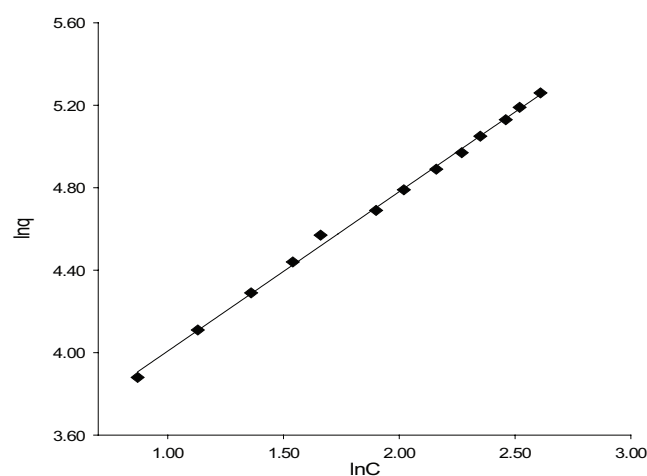


Fig. 10. Freundlich plot of ochratoxin A adsorption on highly porous iron oxide carbon nanocomposite derived from nut shell.

2). The high  $R^2$  value for this isotherm confirmed that Freundlich adsorption isotherm suited the data well as compared to Langmuir isotherm.

### 3.3. Adsorption kinetics

One of the key elements for an adsorbent during adsorption processes is the time of contact needed to attain equilibrium. Fig. 11 indicates that maximum uptake of ochratoxin A take place initially for first few minutes, because more and more free sites are present to adsorb ochratoxin A. With the passage of time maximum free sites are tied up which leads to slow rate of adsorption and at last a point of saturation is reached. At this point curve become parallel to the X-axis and the time at which this point is reached is known as equilibrium time of adsorption. The equilibrium time for ochratoxin A (400 ppm) adsorption on the prepared adsorbent derived from coconut shell was 240 min. The experiments were carried out at pH 7 as at this pH Iron oxide remained in composite structure [29].

Pseudo first order [30] and second order [31] models were applied in order to determine the kinetic constants and order of the adsorption process. The pseudo first order equation is given as follow:

$$\ln(q_e - q) = \ln q_e - k_a t \quad (3)$$

In the above equation,  $q_e$  represents the amount of ochratoxin A adsorption ( $\text{mg}\cdot\text{g}^{-1}$ ) at equilibrium whereas  $q$  denotes the amount of ochratoxin A adsorption ( $\text{mg}\cdot\text{g}^{-1}$ ) at time  $t$  and  $k_a$  ( $\text{min}^{-1}$ ) is the first order rate constant. A straight

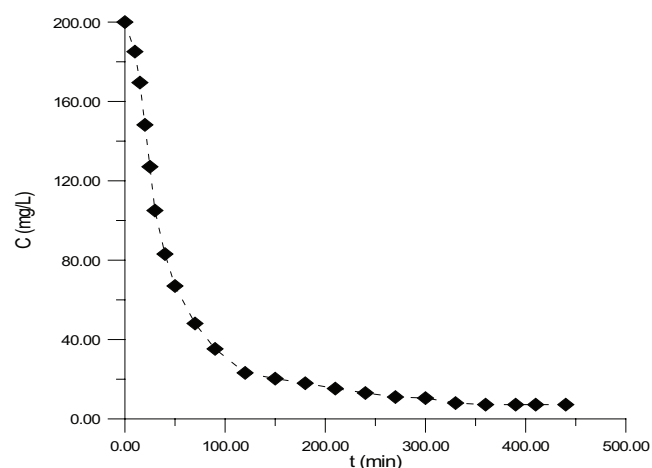


Fig. 11. Effect of contact time of adsorption of ochratoxin A on highly porous Iron oxide carbon nanocomposite derived from coconut shell.

line was obtained when  $\ln(q_e - q)$  was plotted against  $t$  (Fig. 12). The values of  $k_a$  and  $R^2$  are given in Table 3 and were noted to be 0.0174 and 0.993 for ochratoxin A adsorption (400 ppm) at pH 7.

The pseudo second order kinetics equation is represented by the equation:

$$\frac{t}{qt} = \frac{1}{k_2 q^2} + \left(\frac{1}{q}\right)t \quad (4)$$

A straight line was observed, when  $t/q$  was plotted against  $t$  (Fig. 13). Values of  $K_2$  and  $q$  were determined from intercept and slope of this plot. These values along with values of  $R^2$  are summarized in Table 3.

The data in Table 3, indicates that pseudo first order rate equation fits the data well with high correlation coefficient as compared pseudo second kinetic model.

### 3.4. Effect of pH

One of the key element that affect the process of adsorption is pH because it influences the charges, present on the surface of the adsorbent. The degree of ionization of the adsorbate is also affected by the pH. The adsorption potential of the prepared adsorbent at different pH for ochratoxin A is shown in Fig. 14 which indicates that at pH 1–13 the amount of ochratoxin A adsorption is not affected to great extent. The slight decrease in the adsorption at basic pH can be explained on the basis of two probabilities: (i) detachment of iron oxide at acidic pH and (ii) deprotonation of certain functional groups on both adsorbent and adsorbate.

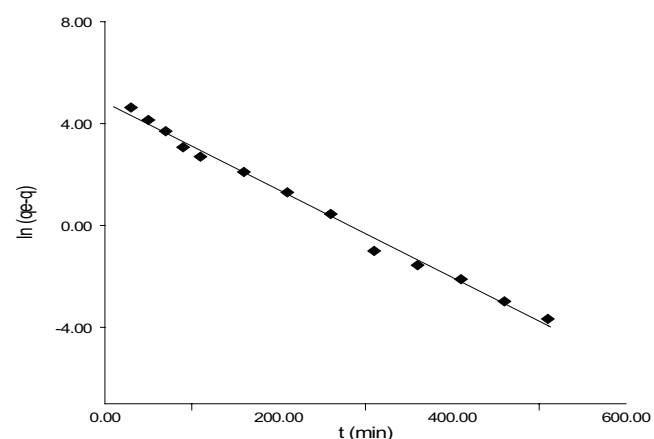


Fig. 12. Pseudo first order kinetics plot for ochratoxin A adsorption on highly porous iron oxide carbon nanocomposite derived from coconut shell.

Table 3

Pseudo first and second order adsorption rate constants and correlation coefficients for the adsorption of ochratoxin A on iron oxide carbon nanocomposites at pH 7

Concentration (ppm)	$q_{e,exp}$ ( $\text{mg}\cdot\text{g}^{-1}$ )	Pseudo first order kinetics model			Pseudo second order kinetics model		
		$K_a$	$R^2$	$q_{e1,cal}$	$K^2$	$R^2$	$q_{e2,cal}$
400	25.9	0.0174	0.993	26.13	0.00112	0.99	15.48

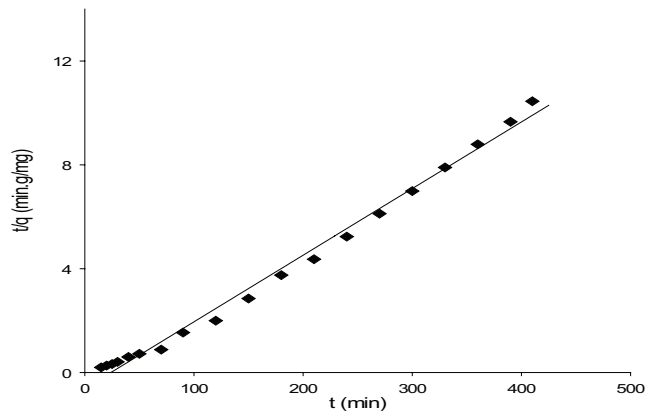


Fig. 13. Pseudo second order kinetics plot for ochratoxin A adsorption on highly porous iron oxide carbon nanocomposite derived from coconut shell.

A slightly high percent adsorption at acidic pH is probably due to the detachment of iron oxide from the composite at acidic pH, that increases the surface area and consequently high percent adsorption have been recorded. From pH 7 to 13 the line is almost straight that indicates that at basic pH the iron oxide remains intact and thus there was no increment in surface area and consequently the percent adsorption was almost same.

Generally the solution pH effect the protonation of poly-functional molecules like ochratoxin A and thus effecting its adsorption. At acidic pH the OH deprotonation is suppressed both in the adsorbent structure (FTIR spectra) and the three ionizable groups in the structure of the ochratoxin A (Fig. 14b) due to which there were positive interaction between the adsorbate and adsorbent. From pH 1 to 5.70 the predominant form the OTA is mostly neutral. However above this pH the monoanionic (5.70 to 8.0), dianionic (8.0 to 11.5) and trianionic (11.5 to 14.0) forms arises. The basic pH deprotonate both the adsorbate and adsorbent.

The repulsion of the negatively charged groups results in the low percent adsorption.

### 3.5. Adsorption thermodynamics

To get insight about the thermodynamic aspects of the adsorption process, the adsorption experiment were carried out at 30, 40, 50 and 60°C respectively. The values of  $\Delta H^\circ$  and  $\Delta S^\circ$  were calculated by applying Vant Hoff equation that is given as under:

$$\ln k = \frac{\Delta S^\circ}{R} - \frac{\Delta H^\circ}{RT} \tag{5}$$

In the above equation  $K$  is the distribution constant of adsorption,  $\Delta H^\circ$  represents the enthalpy change while the entropy change is denoted by  $\Delta S^\circ$ .  $R$  is universal gas con-

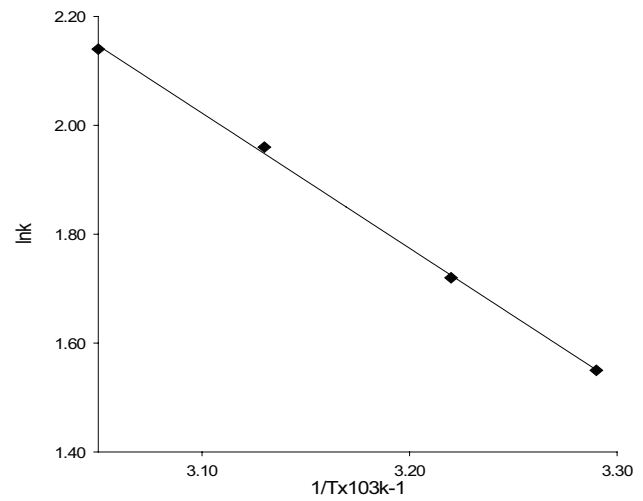


Fig. 15. Vant Hoff plot for adsorption of ochratoxin A on iron oxide carbon nanocomposites prepared from coconut shell.

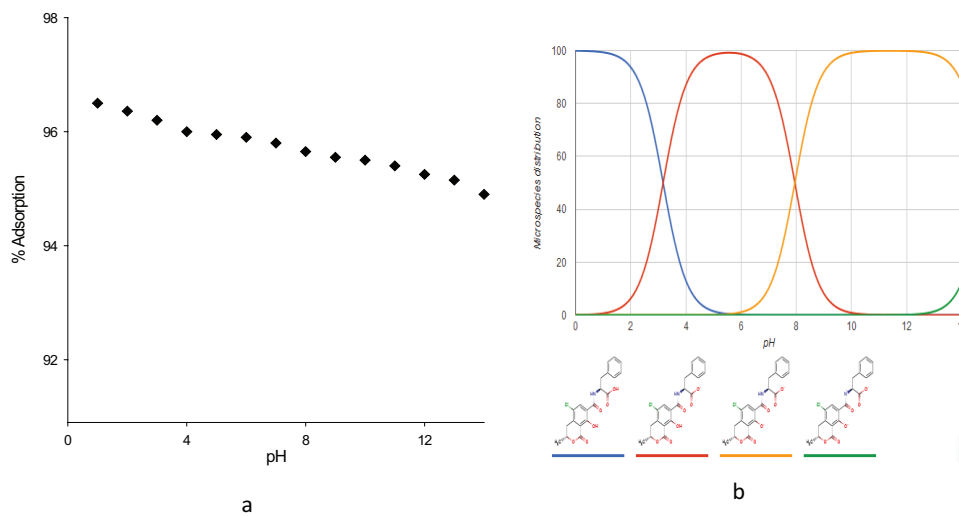


Fig. 14. Effect of pH on ochratoxin A adsorption on highly porous carbon nanocomposite derived from coconut shell (a: % adsorption at different pH. b: micro species distribution diagram).

stant and  $T$  is temperature (in Kelvin).  $\Delta H^\circ$  value was found from the slope whereas the value of  $\Delta S^\circ$  was determined from intercept of the  $\ln K$  and  $1/T$  plot. These values found to be  $-21 \text{ KJ}\cdot\text{mol}^{-1}$  and  $82 \text{ KJ}\cdot\text{mol}^{-1}\cdot\text{deg}^{-1}$  respectively (Fig. 15) for adsorbent, synthesized from coconut shell. The negative value of  $\Delta H^\circ$  shows an exothermic nature of the process. The positive value of  $\Delta S^\circ$  represents an increase in the randomness in the system solid/solution interface.

The value of  $\Delta G^\circ$  (standard free energy) was calculated from the following equation:

$$\Delta G^\circ = \Delta H^\circ - T\Delta S^\circ \quad (6)$$

The values obtained from equation were  $-2.75$ ,  $-3.57$ ,  $-4.39$  and  $-5.21 \text{ KJ}\cdot\text{mol}^{-1}$  at temperature of  $30$ ,  $40$ ,  $50$  and  $60^\circ\text{C}$  respectively. The negative values of  $\Delta G^\circ$  at different temperatures denote the favorable nature of the adsorption process. There is a continuous increase in the value of  $\Delta G^\circ$  with rise in temperature indicating that adsorption is much efficient at elevated temperatures.

#### 4. Conclusion

In the present study highly porous carbon based nanocomposite was synthesized by using coconut shell as a biomass. The prepared nanocomposite was analyzed by using SEM, XRD, TG/DTA, SAA and FTIR which has confirmed the presence of Iron oxide on the surface of the adsorbent. In vitro studies have shown that equilibrium time for highly porous nanostructures prepared from coconut shell at pH 7 was 240 min. However a decline in percent adsorption was observed for the adsorbents at high pH values. The values of  $\Delta H^\circ$  and  $\Delta G^\circ$  were negative while that of  $\Delta S^\circ$  was positive. The increased value of  $\Delta G^\circ$  with temperature demonstrated that the adsorption process was favorable at high temperature. Thus results have revealed that the developed nanostructures can be efficiently utilized as a best substitute for activated powdered carbon to carry out adsorption of ochratoxin A in the alimentary canal of *Gallus domesticus*.

#### References

- [1] P. Bucheli, M.H. Taniwaki, Research on the origin, and on the impact of post-harvest handling and manufacturing on the presence of ochra toxin A in coffee, *Food Addit. Contam.*, 19 (2002) 655–665.
- [2] O.L. Shotwell, C.W. Hesseltine, M.L. Goulden, Ochra toxin A: Occurrence as natural contaminant of a corn sample, *Appl. Microbiol.*, 17 (1969) 765–766.
- [3] G.H.D. Van der Stegen, P.J.M. Essens, J. Van der Lijn, Effect of roasting conditions on reduction of ochra toxin A in coffee, *J. Agric. Food Chem.*, 49 (2001) 4713–4715.
- [4] J. Varga, K. Rigo, B. Toth, J. Teren, Z. Kozakiewicz, Evolutionary relationships among *Aspergillus* species producing economically important myco toxins, *Food Tech. Biotech.*, 11 (2003) 29–36.
- [5] A. Medina, M. Jimenez, R. Mateo, N. Magan, Efficacy of natamycin for control of growth and ochra toxin A production by *Aspergillus carbonarius* strains under different environmental conditions, *J. Appl. Microbiol.*, 103 (2007) 2234–2239.
- [6] X.Q. Chen, K.F. Lam, S.F. Mak, K.L. Yeung, Precious metal recovery by selective adsorption using biosorbents, *J. Hazard. Mater.*, 186 (2011) 902–910.
- [7] A. Gunay, E. Arslankaya, I. Tosun, Lead removal from aqueous solution by natural and pretreated clinoptilolite: adsorption equilibrium and kinetics, *J. Hazard. Mater.*, 146 (2007) 362–371.
- [8] M. Zahoor, F.A. Khan, Adsorption of aflatoxin B1 by magnetic carbon nanocomposite prepared from bagasse, *Arabian J. Chem.*, (2014). In press????.
- [9] S.A. Kahani, M. Hamadian, O. Vandadi, Deposition of magnetite nanoparticles in activated carbons and preparation of magnetic activated carbons. Nano technology and its applications, First Sharjah International Conference, American Institute of Physics, 2007.
- [10] J. Stroka, E. Ankalam, U. Jorissen, J. Gilbert, Immuno-affinity column cleanup with liquid chromatography using post-column bromination for determination of aflatoxins in peanut butter, pistachio paste, fig past, paprika powder. Collaborative study, *J. Assoc. Anal. Chem. Int.*, 83 (2000) 320–340.
- [11] F. Zhang, K.X. Wang, G.D. Li, J.S. Chen, Hierarchical porous carbon derived from rice straw for lithium ion batteries with high-rate performance, *Electro. Chem. Commun.*, 11(1) (2009) 130–133.
- [12] F.A. Khan, M. Zahoor, In vivo detoxification of aflatoxin B1 by magnetic carbon nanostructures prepared from bagasse, *BMC Vet. Res.*, 10 (2014) 255.
- [13] M.M.U.R. Khattak, M. Zahoor, B. Muhammad, Removal of heavy metals from water by carbon nanocomposites prepared from melon wastes, *Desal. Water Treat.*, 75 (2017) 158–173.
- [14] D. Prahas, Y. Kartika, N. Indraswati, S. Ismadji, Activated carbon from jack fruit peel waste by  $\text{H}_3\text{PO}_4$  chemical activation: Pore structure and surface chemistry characterization, *Chem. Eng. J.*, 140 (2008) 32–42.
- [15] L. Li, P.A. Quinlivan, D.R.U. Knappe, Effects of activated carbon surface chemistry and pore structure on the adsorption of organic contaminants from aqueous solution, *Carbon*, 40 (2002) 2085–2100.
- [16] C. Jorge, H. Rios, E.M. Muzquiz, A. Zugasti, D.A. Cortes-Hern, Mechano synthesis as a simple method to obtain a magnetic composite (activated carbon/ $\text{Fe}_3\text{O}_4$ ) form hyper thermia treatment, *J. Bio. Nanomater.*, 7 (2016) 19–28.
- [17] S. Krehula, S. Music, Formation of magnetite in highly alkaline media in the presence of small amounts of ruthenium, *Croatia Chem. Acta.*, 80 (2007) 517–527.
- [18] X. Liu, M. Kim, Solvothermal synthesis and magnetic properties of magnetic Nanoplatelets, *Matt. Lett.*, 63 (2009) 428–430.
- [19] Q. Hengfei, H. Yongkui, L. Siyu, F. Yao, L. Xi, K. Shifei, Synthesis and properties of magnetic carbon nanocages particles for dye removal, *J. Nanomater.*, 2015 (2015) 1–8.
- [20] N.R. Wan, I.M. Wan, A.Y. Mohd, Highly porous carbon materials from biomass by chemical and carbonization method: a comparison study, *J. Chem.*, 46 (2013) 1–6.
- [21] Z. Al-Qodah1, R. Shawabkah, Production and characterization of granular activated sludge, *Brazilian J. Chem. Eng.*, 26 (2009) 127–136.
- [22] H. Deng, L. Yang, G. Tao, J. Dai, Preparation and characterization of activated carbon from cotton stalk by microwave assisted chemical activation, application in methylene blue adsorption from aqueous solution, *J. Hazard. Mater.*, 166 (2009) 1514–1521.
- [23] C. Yanyan, Z. Caineng, M. Maria, H. Suyun, G. Carley, T. Xiaowan, Application of micro-fourier transform infrared spectroscopy (FTIR) in the geological sciences, *Int. J. Mol. Sci.*, 16 (2015) 3023–3025.
- [24] P. Hadi, M. Xu, C.N. Ki, C.S. Lin, G. McKay, A critical review on preparation, characterization and utilization of sludge-derived activated carbons for wastewater treatment, *Chem. Eng. J.*, 260 (2015) 895–906.
- [25] M. Sneha, N.M. Sundaram, Preparation and characterization of an iron oxide-hydroxyapatite nanocomposite for potential bone cancer therapy, *Int. J. Nanomater.*, 10 (2015) 99–106.

- [26] H. Giles, T.H. Macewan, S.N. Nakhwa, D. Smith, Studies in adsorption. part IX. a system of classification of solution adsorption isotherms and its use in diagnosis of adsorption mechanism and its measurement of specific surface areas of solids, *J. Sol. Com.*, 30 (1960) 3973–3993.
- [27] I. Langmuir, The adsorption of gases on plane surfaces of glass mica and platinum, *J. Am. Chem. Soc.*, 40 (1918) 1361–1403.
- [28] H. Freundlich, Über die adsorption in lösungen (Adsorption in solution), *Z. Phys. Chem.*, 57 (1906) 384–470.
- [29] G.H. Wang, C.Y. Xue, F. Chen, Y.L. Ma, X.B. Zhang, Y.Z. Bi, Y.C. Cao, Effects of combinations of ochratoxin A and T-2 toxin on immune function of yellow- feathered broiler chickens, *Poult. Sci.*, 88 (2009) 504–510.
- [30] S. Lagergren, Zur theorie der sogenannten adsorption gelöster stoffe, *K. Sven. Vetensk. akad. Handl.*, 24 (1898) 1–39.
- [31] Y.S. Ho, G. McKay, Pseudo-second order model for sorption processes, *Chem. Eng. J.*, 70 (1999) 115–124.